Research Square

Preprints are preliminary reports that have not undergone peer review.
They should not be considered conclusive, used to inform clinical practice,
or referenced by the media as validated information.

Integrated Multi-omics Links Eph–Ephrin Signaling with Caspase-3 Activation and Hepatic Inflammation in Hypobaric Hypoxia in a Preclinical Model

Sanju Yadav
Institute of Liver and Biliary Sciences
Rupinder Kalra
Banasthali Vidyapith
Gaurav Tripathi
Institute of Liver and Biliary Sciences
Neha Sharma
Institute of Liver and Biliary Sciences
Sushmita Pandey
Institute of Liver and Biliary Sciences
Vipul Sharma
Institute of Liver and Biliary Sciences
Vasundhra Bindal
Institute of Liver and Biliary Sciences
Yash Magar
Institute of Liver and Biliary Sciences
Shimona Ahlawat
Institute of Liver and Biliary Sciences
Ved Prakash Diwedi
International Centre for Genetic Engineering and Biotechnology
Narendra kumar sharma
Banasthali Vidyapith
Nasir Salam
Jamia Millia Islamia
Jaswinder Singh Maras
jassi2param@gmail.com

Institute of Liver and Biliary Sciences

Article

Keywords:

Posted Date: October 8th, 2026

DOI: https://doi.org/10.21203/rs.3.rs-10956360/v1

License: This work is licensed under a Creative Commons Attribution 4.0 International License.
Read Full License

Additional Declarations: No competing interests reported.

Abstract

Background: Acute hypobaric hypoxia causes metabolic stress, disrupts redox balance, and leads to liver injury, but its molecular impact on hepatic function is unclear. This study examined time-dependent liver proteomic and metabolomic changes during acute hypoxia and their links to oncogenic transformation.

Methods: Male SD rats (n=6 per group) were exposed to simulated hypobaric hypoxia at an altitude of 25,000 ft. for durations of 1, 3, or 7 days. Untargeted proteomic and metabolomic analyses were performed on liver tissues to investigate molecular alterations associated with hepatic stress over time. Integrated changes in proteomics and metabolomics were identified and subsequently validated through RT-PCR and immunohistochemistry in liver tissue.

Results: Hypoxia induced significant liver injury, evidenced by elevated serum bilirubin, AST, and ALT levels and a reduced liver-to-body weight ratio ($p<0.05$). Liver metabolomics revealed dynamic time-dependent remodeling at Day1;up-341/Down-20, Day3;up-316/Down-22 and Day7;up-356/Down-10 metabolites as compared to baseline (FC>1.5, $p<0.05$). These metabolite changes were linked to inflammatory and mitochondrial redox metabolism, including tryptophan (C00099, C00025), amino sugar (C00140), folate (C00576), and TCA cycle metabolism (C00025), alongside suppression of nitrogen metabolism (C00262, C00086), suggesting impaired detoxification (>2FC, $p<0.05$). Proteomic analysis showed extensive dysregulation, with Day1;up-1091/down-831, Day3; up-1104/down-821, and Day7; up-453/Down-606 proteins (FC>1.5, $p<0.05$). Enriched proteins were linked to stress responses, lipid and fatty acid metabolism (FADS1, ACOX2, ACOT8, ACADVL, CPT1B), and calcium signaling (PTGS1; >2FC, $p<0.05$). Integrated multiomics revealed strong associations between TCA cycle activation and inflammatory signaling ($R^2>0.7$, $p<0.05$). Network analysis connected apoptosis (BAX, APAF1, CDH1, PRKCD), platelet activation (ATP2B3, PPP2R1B), Eph-ephrin signaling (EPHA7, MYH9, LYN, EPHA3), and angiotensin signaling (ACE, CMA1) with disrupted nucleotide, amino acid, and antioxidant metabolism, highlighting Eph-ephrin signaling as a key mediator of hypoxia-induced hepatic inflammation. RTPCR validation confirmed the dysregulation of these pathways ($p<0.05$). Temporal increase in key genes linked to inflammatory, oxidative, angiogenic and hypoxia linked pathways show significant correlation ($r2>0.9$, $p<0.05$) with liver caspase 3 indicating activation of cell death pathways associated with liver injury due to hypoxia.

Conclusion: Acute hypobaric hypoxia induces early liver injury marked by redox imbalance, metabolic rewiring, and inflammatory activation, with coordinated proteomic metabolomic disruptions highlighting Eph ephrin signalling as a key driver of hypoxia induced hepatic inflammation and a potential therapeutic target.

INTRODUCTION

Hypoxia, which refers to insufficient oxygen reaching the tissues, is a key pathological condition seen in many clinical and environmental situations such as ischemia-reperfusion injury, lung diseases, anemia,

sepsis, and high-altitude exposure (1). Hypobaric hypoxia (HH), specifically associated with high-altitude settings, poses distinct physiological challenges due to lower atmospheric pressure and reduced oxygen partial pressure (2). This leads to disruptions in systemic equilibrium and initiates intricate adaptive and maladaptive responses throughout various organs. Although the liver plays a vital role in metabolism, detoxification, and immune surveillance, its reaction to hypobaric hypoxia has not been studied as extensively as that of the heart and lungs (3).

Studies with rodents in hypobaric chambers have shown substantial liver remodeling and metabolic changes during hypoxia, highlighting how both acute and chronic low oxygen states impact liver function and overall metabolism (5).

The liver has remarkable metabolic flexibility that enables adaptation to fluctuating oxygen levels; however, this same adaptability increases its susceptibility to hypoxia-induced injury (6). Reduced oxygen availability impairs mitochondrial oxidative phosphorylation, leading to decreased ATP generation, disruption of adenine nucleotide balance, and compromised cellular bioenergetics (6). Hypoxia-associated mitochondrial dysfunction also promotes excessive reactive oxygen species (ROS) production, resulting in oxidative damage (7).

A major regulator of the hypoxic response is hypoxia-inducible factor-1α (HIF1α), which coordinates transcriptional adaptation to oxygen deprivation (9). HIF1α activation induces genes involved in angiogenesis, glycolysis, and erythropoiesis, facilitating short-term survival under hypoxic conditions (10). It also upregulated pyruvate dehydrogenase kinase-1 (PDK1), suppressing pyruvate dehydrogenase activity and uncoupling glycolysis from the tricarboxylic acid (TCA) cycle, thereby promoting a shift toward anaerobic glycolysis (11). While these responses support adaptation to acute hypoxia, persistent HIF1α activation contributes to lipid accumulation, redox imbalance, and progression of liver disorders such as nonalcoholic fatty liver disease (NAFLD) and non-alcoholic steato-hepatitis (NASH) (12).

Metabolic reprogramming is a hallmark of hypoxic adaptation, involving disruptions in amino acid, lipid, bile acid, and mitochondrial metabolism that contribute to systemic metabolic imbalance (13). Metabolomic and proteomic approaches have identified hypoxia-associated alterations in metabolites, oxidative stress proteins, inflammatory mediators, and lipid metabolic enzymes (7, 13–16). Inadequate antioxidant defenses exacerbate oxidative damage (17), while activation of NF-κB signaling increases pro-inflammatory cytokines such as IL-6 and TNF-α, promoting hepatocellular injury and disease progression (18, 19). The resulting oxidative stress–inflammation cycle contributes to liver dysfunction. Acute hypobaric hypoxia is known to induce steatosis, inflammation, fibrosis, apoptosis, and elevated ALT/AST levels, reflecting progressive hepatic injury (22–25).

Integrated multi-omics methods have clarified hypoxia-related disease mechanisms (26, 27) by detailing metabolic and proteomic changes. Eph-ephrin signaling, identified as a major pathway, connects hypoxia-driven cell communication, angiogenesis, inflammation, and metabolic reprogramming (28, 29, 35–37). Such multi-omics studies are crucial for showing new molecular mechanisms in hypoxia-induced liver injury. Recent studies have shown changes in liver proteins involved in lipid metabolism,

oxidative defense, and proteostasis, as well as shifts in serum metabolites like HDL, LDL, and amino acids (38) (39). However, early molecular responses of the liver to severe hypobaric hypoxia (> 5,500 m) are still unknown. In this study, male Sprague Dawley rats were subjected to simulated hypobaric hypoxia at an altitude of 25,000 ft (7,620 m) for durations of 1, 3, and 7 days. By integrating proteomic and metabolomic analyses from liver and plasma samples, the aim was to elucidate the molecular alterations associated with early hepatic stress responses during acute hypoxic exposure.

Materials and Methods

Animals and Housing Conditions:

Three month old male Sprague Dawley rats (n = 6 per group; body weight: 250 ± 20 g) were procured from the institutional experimental animal facility. Animals were housed in polypropylene cages under standard laboratory conditions with free access to standard pellet diet and tap water ad libitum. A 12 h light/dark cycle was supported throughout the study at a controlled temperature of 25 ± 1 °C and relative humidity of 55 ± 5%. All environmental conditions, including temperature, humidity, feeding conditions, and housing parameters, were maintained uniformly for both control and experimental groups to minimize experimental variability.

Experimental Design and Acclimatization

Animals were acclimatized for one week prior to experimentation. Before hypoxia exposure, rats were additionally placed in metabolic cages for 24 h at a simulated altitude of 5,000 ft for acclimatization to chamber conditions. Following acclimatization, animals were randomly divided into four groups: baseline normoxic control (Day 0) and hypobaric hypoxia (HH)-exposed groups for Day 1, Day 3, and Day 7 (n = 6 per group).

Hypobaric Hypoxia Exposure:

Hypobaric hypoxia exposure was carried out in a climatic hypoxia chamber maintained at a simulated altitude equivalent to 25,000 ft (320 mmHg). Animals were continuously exposed to hypobaric hypoxia for 1, 3, or 7 days depending on the experimental group. The chamber temperature and humidity were maintained at 25 ± 1 °C and 55 ± 5%, respectively. The measured oxygen concentration inside the chamber was 8.1%, with CO_2 maintained at 524 ppm. The chamber water reservoir remained full to facilitate humidity regulation. Chamber conditions were monitored regularly throughout the experimental duration to ensure stable hypoxic exposure.

Sample Collection:

At the respective experimental endpoints, animals were fasted overnight with free access to water prior to tissue collection. Rats were anesthetized using ketamine hydrochloride (50 mg/kg) and xylazine (5 mg/kg) administered intraperitoneally. Adequate anesthesia was confirmed by loss of pedal reflexes. The liver tissues were excised immediately after sacrifice through a midline abdominal incision. Tissue

samples intended for proteomic and metabolomic analysis were washed with ice-cold phosphate-buffered saline, flash frozen in liquid nitrogen, and stored at -80 °C until further LC -MS/MS analysis.

Ethical Approval:

All experimental procedures were performed in accordance with the guidelines of the Institutional Animal Ethics Committee guidelines for the care and use of laboratory animals institute is Banasthali Vidyapith University, approved ethical committee Bioscience & Biotechnology, Banasthali vidyapith, Rajasthan & ethical number BV/IAEC/2023/4643.

Protein Extraction and Digestion

Frozen liver tissues were pulverized in liquid nitrogen and lysed in RIPA buffer. Lysates were sonicated (3 cycles of 10 seconds on/off, amplitude 30%) and clarified by centrifugation. Total protein concentration was measured, and 1 mg per sample was used for proteomic analysis. Proteins were reduced with 10 mM dithiothreitol (DTT) at 60°C for 1 hour, alkylated with 10 mM iodoacetamide in the dark at room temperature, and digested overnight with sequencing grade trypsin (Promega, V5280). The resulting peptides were desalted using C18 spin columns before LCMS/MS analysis.

Mass Spectrometry Analysis

Peptide samples were analyzed using nano electrospray tandem mass spectrometry (QExactive™ Plus, Thermo Fisher Scientific). Samples were first loaded onto a trap column (75 µm × 2 cm, 3 µm, 100Å, PepMap™ 100) at 8 µL/min, and subsequently separated on an analytical column (75 µm × 25 cm, 2 µm, 100Å, PepMap™ RSLC) using a 120minute gradient of 3 95% buffer B (80% acetonitrile in 0.1% formic acid) at a flow rate of 300 nL/min. MS spectra were acquired in the Orbitrap analyzer at a resolution of 70,000 across an m/z range of 200-2000 using collision induced dissociation (CIDs).

Proteomics Data Analysis

Raw MS/MS data were processed using Proteome Discoverer software (v2.3, Thermo Fisher) against the rat reference proteome. Peptide identification was carried out using Mascot and Amanda search engines with the ptmRS pipeline. Filtering criteria included $p < 0.05$, $q < 0.05$, and FDR < 1%. Only high confidence peptides (rank1, PSMs >3) were retained for analysis.

Metabolite Extraction and Metabolomics Analysis

Metabolites were extracted from liver tissue using an organic phase extraction protocol. Samples were analyzed via LCMS in both positive and negative ion modes. Metabolite identification was performed based on accurate mass to charge ratios (m/z), MS/MS fragmentation patterns, and isotopic distribution by referencing HMDB, KEGG, and an inhouse custom database. Peaks with more than 50% missing values (ion intensity = 0) were excluded, and remaining zeros were imputed with half the minimum

detected value. Only metabolites with confirmed annotations were included. The datasets from both ion modes were merged, and the resulting matrix was analyzed using MetaboAnalyst 6.0.

Histopathological and Fibrosis Assessment by Hematoxylin Eosin and Sirius Red Staining.

Liver tissues were collected post-sacrifice and fixed in 10% neutral buffered formalin for 24–48 hours before graded alcohol dehydration, xylene clearing, and paraffin embedding. Sections (4–5 µm) were cut using a rotary microtome and placed on glass slides.

For H&E staining, sections were deparaffinized, rehydrated through descending ethanol concentrations, stained with hematoxylin, differentiated, counterstained with eosin, dehydrated, cleared in xylene, and mounted with DPX. Slides were evaluated for histopathological changes including hepatocellular degeneration, steatosis, inflammation, sinusoidal dilatation, and structural disruption. Sirius Red staining followed similar preparation, with sections stained in 0.1% Sirius Red (picric acid), washed with acetic acid, dehydrated, cleared in xylene, and mounted. Collagen fibers and fibrotic regions appeared red. Images were captured with a light microscope. Steatosis and fibrosis were qualitatively assessed, while fibrosis area percentage was quantified using ImageJ software, comparing Sirius Red-positive collagen to total tissue area.

Immunohistochemistry for Caspase-3

Immunohistochemical staining for Caspase-3 was performed on paraffin-embedded liver sections (4-5 µm). Briefly, sections were deparaffinized, rehydrated, and subjected to antigen retrieval in citrate buffer (pH 6.0). Endogenous peroxidase activity was blocked using 3% H_2O_2 followed by blocking with 5% BSA. Sections were incubated overnight at 4°C with primary antibody against Caspase-3, followed by HRP conjugated secondary antibody incubation. Immunoreactivity was visualized using DAB chromogen and counterstained with hematoxylin. Stained sections were examined under a light microscope and representative images were captured. Quantitative analysis of DAB positive staining was performed using ImageJ software.

Additionally, to systematically confirmed molecular changes liver changes across time points, a separate cohort of rats per group was exposed to hypobaric hypoxia for 1, 3, and 7 days. Liver samples were collected and processed.

Data Analysis and Pathway Integration

Metabolomics and proteomics data were processed and analyzed using MetaboAnalyst 6.0. Intensity normalization and Pareto scaling adjusted for feature variance, followed by pattern recognition to assess liver profiles across groups. Principal Component Analysis (PCA) visualized sample groupings, while Partial Least Squares Discriminant Analysis (PLSDA) modeled expression profiles and validated prediction with leave-one-out cross-validation; R^2 and Q^2 metrics were calculated. Weighted PLS regression identified the top 20 discriminatory features, which were annotated as metabolites and proteins.

Weighted Gene Co-expression Network Analysis (WGCNA) integrated metabolite concentrations with proteomic data to examine functional relationships and temporal changes during hypoxia. Statistical significance was set at $p<0.05$.

Pathway enrichment and topology analysis used normalized values in MetaboAnalyst 6.0. Metabolites were mapped via the Rattus norvegicus KEGG database(1), and Enrichr identified enriched pathways in proteomics ($p<0.05$).

Statistical Analysis

Statistical analysis was performed using GraphPad Prism version 8 and SPSS version 26; $p<0.05$ using Benjamini-Hochberg correction were considered significant. Results are shown as mean and SD unless indicated otherwise. Unpaired (two-tailed) Student's t test and the Mann-Whitney U test were performed for two-groups comparison. For comparison among more than two groups, one-way ANOVA and the Kruskal-Wallis's test were performed. All correlations were performed using Spearman correlation analysis, and $r2>0.5$ and $p<0.05$ were considered significant.

Results

Experimental design and impact of hypobaric hypoxia from day 1 to day 7 on rat liver

This study examined molecular alterations in rat livers following exposure to hypobaric hypoxia at 25,000 ft (320 mmHg) for durations of 1, 3, or 7 days, under controlled temperature and humidity conditions. After an overnight fast, liver tissues were collected for histopathological, proteomic, and metabolomic analyses as described in Figure 1A. Food and water consumption, as well as body weight, showed significant decreases after 7 days of hypobaric hypoxia exposure (Figure 1B). Notably, AST and ALT levels showed mild elevations alongside a marked increase in hepatic fat accumulation and inflammatory neutrophil infiltration on day 7 (Figure 1B and Figure 1C).

Liver Metabolomics Revealed Distinct Hepatic Metabolic Alterations During Hypobaric Hypoxia.

The flowchart depicts the comprehensive experimental workflow encompassing hypoxia exposure, liver tissue collection, metabolomics analysis, and identification of differentially regulated metabolites (Figure-2A). Partial least squares discriminant analysis (PLS-DA) revealed a clear distinction between normoxic controls and hypoxia-exposed groups, underscoring significant changes in hepatic metabolic profiles following hypobaric hypoxia (Figure-2B). The progressive separation seen among Day 1, Day 3, and Day 7 cohorts shows duration-dependent metabolic adaptation during hypoxic stress. Heatmap analysis highlighted distinct patterns of metabolite expression across all experimental groups (Figure-2C). Differential metabolite analysis (Volcano plot) revealed pronounced metabolic perturbations corresponding to varying durations of hypoxia exposure. Specifically, Day 1 hypoxia resulted in 341 up- and 20 downregulated metabolites, Day 3 showed 316 upregulated and 22 downregulated metabolites; and Day 7 showed the greatest level of metabolic disruption with 356 upregulated and 31 downregulated

metabolites (Figure-2D). Venn diagrams showed that metabolites significantly upregulated under hypoxia were linked to methionine and cysteine metabolism, glutathione metabolism, thiamine metabolism, malate-aspartate shuttle, citrate cycle (TCA cycle), pyrimidine metabolism, and purine metabolism pathways (Figure-2E, $p<0.05$). Conversely, downregulated metabolites were associated with taurine and hypotaurine metabolism, bile acid biosynthesis, histidine metabolism, beta-alanine metabolism, methyl histidine metabolism, and ammonia recycling pathways ($p<0.05$) (Figure-2E). Mean decrease in accuracy analysis showed several metabolites correlating with hypoxia exposure (Figure-2F). Receiver operating characteristic (ROC) analysis showed high predictive accuracy for the selected metabolite panel in distinguishing hypoxia-exposed groups from controls, suggesting their potential as biomarkers for hypoxia-induced hepatic metabolic dysfunction (Figure-2F). In summary, these results show that hypobaric hypoxia induces significant, time-dependent metabolic reprogramming in rat liver tissue, characterized by alterations in amino acid metabolism, energy metabolism, redox equilibrium, nucleotide metabolism, and bile acid-associated metabolic pathways.

Liver Proteomics analysis Revealed Distinct Hepatic Metabolic Alterations During Hypobaric Hypoxia.

The flowchart depicts the study design, including a comparative analysis of liver proteins, identification of differential regulated proteins and their functional significance (Figure-3A). PLS-DA analysis showed clear separation between normoxic controls and groups exposed to hypoxia, highlighting notable changes in hepatic protein profiles after hypobaric hypoxia (Figure-3B). Hierarchical clustering revealed unique patterns of protein expression in each experimental group (Figure-3C). Differentially expressed proteins (Volcano plot) during hypoxia: Day 1 exposure led to 1091 up- and 331 downregulated proteins, Day 3 resulted in 1146 up- and 472 downregulated proteins, and Day 7 showed 453 up- and 606 downregulated proteins, reflecting progressive proteome changes with continued hypoxia ($FC>1.5$, $p<0.05$, $FDR<0.01$, Figure-3D). Comparative pathway enrichment showed pathways affected by hypoxia the upregulated proteins were related to metabolic processes, oxidative phosphorylation, glutathione metabolism, fatty acid degradation, pyruvate and amino acid metabolism, pentose phosphate pathway, ribosome biogenesis, thermogenesis, carbon metabolism, proteasome activity, and several neurodegenerative disease pathways (Figure-3E, $p<0.05$). Whereas the downregulated proteins were linked to lysosomal function, bile secretion, focal adhesion, actin cytoskeleton regulation, protein digestion and absorption, extracellular matrix-receptor interactions, endocytosis, complement and coagulation cascades, and multiple amino acid metabolism pathways (valine, leucine, isoleucine degradation, tryptophan, histidine, and arginine biosynthesis, $p<0.05$, Figure-3E) respectively. Analysis of mean decrease in accuracy pinpointed specific proteins associated with hypoxia (Figure-3F). ROC analyses showed robust predictive capability for the chosen protein panel with high $AUC>0.9$,$p<0.05$. Overall, liver proteomics results show that hypobaric hypoxia causes marked and time-dependent remodeling of the liver proteome, towards more pathogenic and inflammatory kind specifically influencing mitochondrial metabolism, oxidative stress response, amino acid and energy metabolisms, cytoskeletal structure, extracellular matrix regulation, platelet degranulation, neutrophil degradation, and hypoxia-related signal pathways.

Analysis of the liver proteome and metabolome shows that hypobaric hypoxia significantly affects inflammation, oxidative stress, angiogenesis, and lipid metabolism.

To understand the metabolic disturbances linked to hypobaric hypoxia (associated with temporal disease progression). The proteomics and metabolomics data were subjected to integration analysis (Figure-4A). We used two independent strategies to integrate the multi-omics data. 1) for temporal integration: The proteomics and metabolomics data was subjected to correl analysis (day1 to day 7) to identify proteins and metabolites that correlate ($R2>0.7$, $p<0.05$) with the days to exposure. We also performed weighted proteome /metabolome correlation network analysis (WP/MCNA) and show metabolite and proteins cluster specific to day of exposure (hypobaric hypoxia).

The correl analysis of proteomics and metabolomics shows temporal disease progression throughout hypoxia (Figure-4B). Proteins which positively correlated to the increase in hypobaric hypoxia condition were significantly linked to valine degradation, protein citrullination, post-translational modification, immune response, intracellular signaling, and metabolic processes and metabolomic enrichment analysis showed increased involvement of glutamate metabolism, purine metabolism, ketone body metabolism, tryptophan metabolism, phenylalanine metabolism, and amino acid metabolic pathways whereas proteins and metabolites which showed negative correlation with the temporal change in hypoxia exposure were linked to ammonia recycling, beta-alanine metabolism, histidine metabolism and other pathways (Figure-4C).

Multiomics integration using temporal association analysis and weighted protein co-expression network analysis (WGCNA) revealed distinct metabolite and protein modules, which were further connected through regulatory network mapping to identify functionally associated pathways. The mean cluster intensity (MCI) analysis demonstrated temporal changes in both proteomic and metabolomic datasets from Day 0 to Day 7 of hypoxia exposure (Figure 4D).

Distinct clustering patterns among metabolomic and proteomic modules across different time points were identified, Day 7 hypoxia was specific to MEblue module for the metabolite and MEgreen, MEblack, MEmegenta, MEyello, and MEblue for the protein module respectively (Figure 4D).

The identified metabolite and proteins modules were cross correlated to identified proteins and metabolite integration and linked pathways. We observed strong positive and negative associations among proteomic and metabolomic modules (Figure-4E). MEblue module for the metabolite showed strong correlation with MEgreen, MEblack, MEmegenta, MEyello, and MEblue for the protein module specific to day 7, integrated network analysis of these module showed significant correlation of the metabolites and proteins linked to amino acid metabolism, platelet activation, angiogenesis, apoptosis, EGFR signaling, and lipid metabolism (Figure 4F). Key metabolites including pyruvate, glutamate, folate-associated metabolites, betaine aldehyde, and amino acid intermediates displayed strong associations with proteins linked to platelet activation, apoptosis signaling, and metabolic regulation. These findings shows that hypobaric hypoxia even by day 7 induces coordinated proteomic and metabolomic remodeling, associated to induction of apoptosis, inflammatory and oxidative changes, which

contributes to significant increase in the lipid accumulation in the liver (metabolic stress) and thus induces molecular derangement in the liver (Figure 4F). These pathways are crucial and warrants validation and association to pathological transformation due to hypoxia.

Hypoxia-induced inflammation and oxidation correlate with liver caspase 3 levels: molecular validation

The molecular pathways identified through the integration of proteomic and metabolomic analyses were then confirmed in an independent cohort of rats subjected to hypobaric hypoxia (Figure-5A). Major pathways revealed by multiomics integration were corroborated using RT-PCR and immunohistochemistry (IHC) methodologies.

Metabolomic analysis revealed progressively increased activity in metabolic pathways such as amino sugar, betaine, pyridoxine, and folate metabolism from Day 0 to Day 7 of hypoxic exposure (Figure-5B). Key metabolites (e.g., C00140, C00025, C00576, HMDB0002031) were significantly more abundant by Day 7, reflecting substantial metabolic reprogramming (Figure-5B).

Proteomic pathway analysis showed activation of apoptosis, fatty acid metabolism, platelet homeostasis, ephrin signaling, and angiotensinogen pathways (key proteins temporally increased from Day1 to Day7 Figure-5C). Immunohistochemical analysis showed a progressive increase in Caspase-3 expression during hypoxic exposure (Day1to Day7, Figure-5D). Minimal staining was noted at Day 0 and Day 1, while robust positive staining appeared at Day 3 and Day7, signifying enhanced apoptotic activity with increase in hypoxia exposure

Interestingly RT-qPCR validation also confirmed substantial upregulation of multiple genes associated with hypoxia, inflammation, apoptosis, angiogenesis, and metabolic regulation (Figure 5E). Genes including GALE, BCL2, NF-KB, RAB10, VEGF, IL6, HIF, TYMP, EPO, CLSTN1, SOD1, SOD2, NOX4, DEPCDT, and VEGF demonstrated increasing fold expression over the experimental timeline, with maximal induction frequently observed at Day 7 (Figure-5E). Finally, liver expression of caspase 3 showed direct correlation ($r^2>0.85$, $p<0.05$) with genes linked to apoptotic signaling, hypoxia-responsive pathways, oxidative stress markers, angiogenesis-related proteins, and inflammatory mediators, showing tightly coordinated molecular regulation during hypoxia-induced progression (Figure 5F). These results support the combined proteomic and metabolomic data, highlighting broad metabolic, apoptotic, inflammatory, and angiogenic changes under hypoxia.

Discussion

Hypobaric hypoxia is marked by reduced pressure and oxygen, affects both gut and brain function (1). It alters gut metabolism, impacting nutrient absorption and digestion, in addition the brain faces oxidative changes, which may impair cognition. These effects show hypobaric hypoxia's role in multi-organ dysfunction beyond liver injury (2, 3). The liver is particularly susceptible to oxygen deprivation because of its high metabolic activity and dependence on mitochondrial oxidative phosphorylation for maintenance of cellular energy homeostasis (4).

In this study, rats were subjected to hypobaric hypoxia for seven days, after which physiological, biochemical, histopathological, metabolomic, proteomic, and molecular alterations in liver tissue were assessed. Exposure to hypobaric hypoxia resulted in a significant decrease in body weight and food intake, indicating a disruption in systemic energy balance under oxygen-deficient conditions. These findings are consistent with previous research demonstrating that hypoxia suppresses appetite and modifies nutrient utilization via hypoxia-inducible signaling pathways and neuroendocrine mechanisms (43). The combination of reduced caloric intake and heightened metabolic demand during hypoxic stress likely contributes to the observed impairment in body weight gain; similar decreases in body weight and feeding behavior have been documented in experimental high-altitude hypoxia models (43).

Biochemical analyses showed that serum AST and ALT levels increased after exposure to hypoxia, pointing to liver cell injury and compromised membrane integrity. Elevated transaminase activity is recognized as an indicator of liver damage linked to oxidative stress, mitochondrial dysfunction, and inflammation (44). Hypoxia impairs mitochondrial respiratory function, leading to excess reactive oxygen species (ROS), lipid peroxidation, and destabilized membranes, which causes intracellular enzymes to leak into the bloodstream (45). Continued rises in AST and ALT during extended hypoxia suggest ongoing liver injury and worsening cellular health. Histopathological results using H&E staining revealed advancing hepatic steatosis, liver cell degeneration, sinusoidal dilation, inflammatory infiltration, and disrupted liver structure in groups exposed to hypoxia. This hypoxia-induced steatosis may be due to changes in lipid metabolism, defective mitochondrial β oxidation, oxidative stress, and HIF-driven activation of lipogenic pathways (46). Sirius Red (SR) staining also showed increasing collagen buildup and extracellular matrix accumulation in the livers exposed to hypoxia, marking the activation of fibrotic pathways under sustained low-oxygen conditions. Prior studies have shown that hypoxia activates hepatic stellate cells through HIF 1α signaling, ROS production, inflammatory cytokines, and TGF β pathways, resulting in more collagen synthesis and fibrotic changes (22, 47). Current proteomics data further confirm these findings, indicating altered extracellular matrix organization, focal adhesion, and cytoskeletal pathways, supporting evidence of structural remodeling in the liver during hypoxia.

Liver metabolomics analysis showed substantial hepatic metabolic reprogramming during exposure to hypobaric hypoxia. Multivariate statistical analyses indicated pronounced segregation between normoxia and hypoxia-treated groups, underscoring significant alterations in hepatic metabolic profiles resulting from oxygen deprivation. Comparable metabolic divergence has been documented in previous studies of chronic hypoxia (48). Differential metabolite analysis revealed significant enrichment in pathways including methionine and cysteine metabolism, glutathione metabolism, thiamine metabolism, malate-aspartate shuttle, citrate cycle, purine metabolism, and pyrimidine metabolism. Hypoxia-induced mitochondrial dysfunction is associated with impaired electron transport chain activity and increased ROS production, leading to oxidative stress and metabolic imbalance (49). The activation of glutathione metabolism observed represents a compensatory antioxidant response aimed at neutralizing excessive ROS accumulation and maintaining intracellular redox homeostasis. Enhanced methionine and cysteine metabolism further supports increased glutathione biosynthesis during hypoxic stress, as cysteine serves as the rate-limiting substrate for glutathione synthesis (50). Alterations in malate-aspartate

shuttle and tricarboxylic acid cycle pathways suggest significant mitochondrial metabolic rewiring and impaired oxidative phosphorylation under oxygen-deficient conditions (51). Taurine and related metabolic pathways, as well as bile acid biosynthesis, beta alanine, histidine metabolism, and ammonia recycling, were downregulated under 7- days of hypoxia. Taurine is vital for membrane stability, mitochondrial function, calcium balance, and anti-oxidative defense; its suppression may increase vulnerability to oxidative damage and liver dysfunction (5).

Liver Proteomics analysis showed substantial alterations in hepatic protein expression, notably an upregulation of proteins related to glycolysis, the pentose phosphate pathway, and proteasome activity. These findings suggest mitochondrial dysfunction and an adaptive shift in cellular energy metabolism. Hypoxic conditions restrict mitochondrial respiration, increasing cellular dependence on glycolysis and activating protein quality control mechanisms such as the ubiquitin-proteasome system. The concurrent elevation of antioxidant and proteostasis-associated proteins shows a coordinated hepatic response to oxidative stress. Additionally, proteomic profiling revealed enrichment of pathways associated with mitochondrial dysfunction, oxidative stress, disrupted proteostasis, and metabolic imbalance, all of which are common cellular outcomes of hypoxic injury (52). Earlier proteomics studies under chronic hypoxia (48) have reported similar enrichment of neurodegeneration-related molecular pathways.

Downregulated proteins observed in the present study were linked to lysosomal function, focal adhesion, extracellular matrix organization, actin cytoskeleton regulation, endocytosis, complement activation, and protein digestion and absorption processes. Hypoxia-induced disturbances of cytoskeletal architecture and extracellular matrix stability contribute to hepatic cell injury, vascular dysfunction, inflammation, and progression of fibrosis (53). Reduced expression of proteins involved in focal adhesion and cytoskeletal maintenance may compromise hepatic structural integrity during prolonged hypoxic exposure.

Integrated proteomic and metabolomic analyses showed proteins and metabolites that strongly correlate with increased hypoxia exposure, especially at Day 7. Positively correlated proteins were linked to amino acid metabolism, immune response, and intracellular signaling, while negatively correlated molecules were associated with ammonia recycling and histidine metabolism. Network mapping revealed distinct modules tied to apoptosis, angiogenesis, platelet activation, and lipid metabolism. Key metabolites like pyruvate and glutamate connected with protein markers for platelet activation and metabolic regulation. Overall, hypobaric hypoxia triggered coordinated molecular changes related to apoptosis, inflammation, oxidative stress, and lipid accumulation in the liver which warrants validation.

LCMS/MS, immune-histochemical, and RTPCR methods validated metabolites and proteins involved in relevant pathways. Caspase 3 showed increased expression in hypoxia-treated groups, signifying apoptotic activation. As a key mitochondrial protease, Caspase 3 is activated by oxidative stress, mitochondrial damage, inflammation, and cytochrome c release (54). Metabolomics and proteomics findings were substantiated by RT PCR and Caspase 3 immunohistochemistry, which showed significant changes in hypoxia-responsive genes linked to oxidative stress, inflammation, angiogenesis,

mitochondrial dysfunction, and apoptosis. Collectively, the increase in apoptosis-related gene expression and Caspase 3 activity points to programmed cell death during hypoxia-induced liver injury.

Finally our study shows that short term hypobaric hypoxia causes progressive liver injury marked by metabolic dysfunction, oxidative stress, mitochondrial damage, inflammation, apoptosis, and changes in the extracellular matrix. Combined analyses offer detailed insight into liver adaptation and damage under ongoing low-oxygen conditions. These results point to key areas for further research and improvement in Hypoxia induced liver injury.

Declarations

Conflict of interest statement:

All authors have declared no conflict of interest.

Financial support

The work was supported by LSRB/01/15001/LSRB-420/PEE&BS/2024 LSRB, Defence Research and Development Organisation (DRDO).

Background

Acute hypobaric hypoxia causes metabolic stress, disrupts redox balance, and leads to liver injury, but its molecular impact on hepatic function is unclear. This study examined time-dependent liver proteomic and metabolomic changes during acute hypoxia and their links to oncogenic transformation.

Methods

Male SD rats (n = 6 per group) were exposed to simulated hypobaric hypoxia at an altitude of 25,000 ft. for durations of 1, 3, or 7 days. Untargeted proteomic and metabolomic analyses were performed on liver tissues to investigate molecular alterations associated with hepatic stress over time. Integrated changes in proteomics and metabolomics were identified and subsequently validated through RT-PCR and immunohistochemistry in liver tissue.

Results

Hypoxia induced significant liver injury, evidenced by elevated serum bilirubin, AST, and ALT levels and a reduced liver-to-body weight ratio ($p < 0.05$). Liver metabolomics revealed dynamic time-dependent remodeling at Day1;up-341/Down-20, Day3;up-316/Down-22 and Day7;up-356/Down-10 metabolites as compared to baseline (FC > 1.5, $p < 0.05$). These metabolite changes were linked to inflammatory and mitochondrial redox metabolism, including tryptophan (C00099, C00025), amino sugar (C00140), folate (C00576), and TCA cycle metabolism (C00025), alongside suppression of nitrogen metabolism (C00262, C00086), suggesting impaired detoxification (> 2FC, $p < 0.05$). Proteomic analysis showed extensive

dysregulation, with Day1;up-1091/down-831, Day3; up-1104/down-821, and Day7; up-453/Down-606 proteins (FC > 1.5, $p < 0.05$). Enriched proteins were linked to stress responses, lipid and fatty acid metabolism (FADS1, ACOX2, ACOT8, ACADVL, CPT1B), and calcium signaling (PTGS1; >2FC, $p < 0.05$). Integrated multiomics revealed strong associations between TCA cycle activation and inflammatory signaling ($R^2>0.7$, $p < 0.05$). Network analysis connected apoptosis (BAX, APAF1, CDH1, PRKCD), platelet activation (ATP2B3, PPP2R1B), Eph-ephrin signaling (EPHA7, MYH9, LYN, EPHA3), and angiotensin signaling (ACE, CMA1) with disrupted nucleotide, amino acid, and antioxidant metabolism, highlighting Eph-ephrin signaling as a key mediator of hypoxia-induced hepatic inflammation. RTPCR validation confirmed the dysregulation of these pathways ($p < 0.05$). Temporal increase in key genes linked to inflammatory, oxidative, angiogenic and hypoxia linked pathways show significant correlation ($r2 > 0.9$, $p < 0.05$) with liver caspase 3 indicating activation of cell death pathways associated with liver injury due to hypoxia.

Ethical Approval:

All experimental procedures were performed in accordance with the guidelines of the Institutional Animal Ethics Committee guidelines for the care and use of laboratory animals institute is Banasthali Vidyapith University, approved ethical committee Bioscience & Biotechnology, Banasthali vidyapith, Rajasthan & ethical number BV/IAEC/2023/4643.

Protein Extraction and Digestion

Frozen liver tissues were pulverized in liquid nitrogen and lysed in RIPA buffer. Lysates were sonicated (3 cycles of 10 seconds on/off, amplitude 30%) and clarified by centrifugation. Total protein concentration was measured, and 1 mg per sample was used for proteomic analysis. Proteins were reduced with 10 mM dithiothreitol (DTT) at 60°C for 1 hour, alkylated with 10 mM iodoacetamide in the dark at room temperature, and digested overnight with sequencing grade trypsin (Promega, V5280). The resulting peptides were desalted using C18 spin columns before LCMS/MS analysis.

Mass Spectrometry Analysis

Peptide samples were analyzed using nano electrospray tandem mass spectrometry (QExactive™ Plus, Thermo Fisher Scientific). Samples were first loaded onto a trap column (75 µm × 2 cm, 3 µm, 100Å, PepMap™ 100) at 8 µL/min, and subsequently separated on an analytical column (75 µm × 25 cm, 2 µm, 100Å, PepMap™ RSLC) using a 120minute gradient of 3 95% buffer B (80% acetonitrile in 0.1% formic acid) at a flow rate of 300 nL/min. MS spectra were acquired in the Orbitrap analyzer at a resolution of 70,000 across an m/z range of 200–2000 using collision induced dissociation (CIDs).

Proteomics Data Analysis

Raw MS/MS data were processed using Proteome Discoverer software (v2.3, Thermo Fisher) against the rat reference proteome. Peptide identification was carried out using Mascot and Amanda search engines with the ptmRS pipeline. Filtering criteria included $p < 0.05$, $q < 0.05$, and FDR < 1%. Only high confidence peptides (rank1, PSMs > 3) were retained for analysis.

Metabolite Extraction and Metabolomics Analysis

Metabolites were extracted from liver tissue using an organic phase extraction protocol. Samples were analyzed via LCMS in both positive and negative ion modes. Metabolite identification was performed based on accurate mass to charge ratios (m/z), MS/MS fragmentation patterns, and isotopic distribution by referencing HMDB, KEGG, and an inhouse custom database. Peaks with more than 50% missing values (ion intensity = 0) were excluded, and remaining zeros were imputed with half the minimum detected value. Only metabolites with confirmed annotations were included. The datasets from both ion modes were merged, and the resulting matrix was analyzed using MetaboAnalyst 6.0.

Histopathological and Fibrosis Assessment by Hematoxylin Eosin and Sirius Red Staining.

Liver tissues were collected post-sacrifice and fixed in 10% neutral buffered formalin for 24–48 hours before graded alcohol dehydration, xylene clearing, and paraffin embedding. Sections (4–5 µm) were cut using a rotary microtome and placed on glass slides.For H&E staining, sections were deparaffinized, rehydrated through descending ethanol concentrations, stained with hematoxylin, differentiated, counterstained with eosin, dehydrated, cleared in xylene, and mounted with DPX. Slides were evaluated for histopathological changes including hepatocellular degeneration, steatosis, inflammation, sinusoidal dilatation, and structural disruption. Sirius Red staining followed similar preparation, with sections stained in 0.1% Sirius Red (picric acid), washed with acetic acid, dehydrated, cleared in xylene, and mounted. Collagen fibers and fibrotic regions appeared red. Images were captured with a light microscope. Steatosis and fibrosis were qualitatively assessed, while fibrosis area percentage was quantified using ImageJ software, comparing Sirius Red-positive collagen to total tissue area.

Immunohistochemistry for Caspase-3

Immunohistochemical staining for Caspase-3 was performed on paraffin-embedded liver sections (4–5 µm). Briefly, sections were deparaffinized, rehydrated, and subjected to antigen retrieval in citrate buffer (pH 6.0). Endogenous peroxidase activity was blocked using 3% H_2O_2 followed by blocking with 5% BSA. Sections were incubated overnight at 4°C with primary antibody against Caspase-3, followed by HRP conjugated secondary antibody incubation. Immunoreactivity was visualized using DAB chromogen and counterstained with hematoxylin. Stained sections were examined under a light microscope and representative images were captured. Quantitative analysis of DAB positive staining was performed using ImageJ software.

Additionally, to systematically confirmed molecular changes liver changes across time points, a separate cohort of rats per group was exposed to hypobaric hypoxia for 1, 3, and 7 days. Liver samples were

collected and processed.

Data Analysis and Pathway Integration

Metabolomics and proteomics data were processed and analyzed using MetaboAnalyst 6.0. Intensity normalization and Pareto scaling adjusted for feature variance, followed by pattern recognition to assess liver profiles across groups. Principal Component Analysis (PCA) visualized sample groupings, while Partial Least Squares Discriminant Analysis (PLSDA) modeled expression profiles and validated prediction with leave-one-out cross-validation; R^2 and Q^2 metrics were calculated. Weighted PLS regression identified the top 20 discriminatory features, which were annotated as metabolites and proteins.

Weighted Gene Co-expression Network Analysis (WGCNA) integrated metabolite concentrations with proteomic data to examine functional relationships and temporal changes during hypoxia. Statistical significance was set at $p < 0.05$.

Pathway enrichment and topology analysis used normalized values in MetaboAnalyst 6.0. Metabolites were mapped via the Rattus norvegicus KEGG database(1), and Enrichr identified enriched pathways in proteomics ($p < 0.05$).

Statistical Analysis

Statistical analysis was performed using GraphPad Prism version 8 and SPSS version 26; $p < 0.05$ using Benjamini-Hochberg correction were considered significant. Results are shown as mean and SD unless indicated otherwise. Unpaired (two-tailed) Student's t test and the Mann-Whitney U test were performed for two-groups comparison. For comparison among more than two groups, one-way ANOVA and the Kruskal-Wallis's test were performed. All correlations were performed using Spearman correlation analysis, and $r2 > 0.5$ and $p < 0.05$ were considered significant.

Results:

Experimental design and impact of hypobaric hypoxia from day 1 to day 7 on rat liver

This study examined molecular alterations in rat livers following exposure to hypobaric hypoxia at 25,000 ft (320 mmHg) for durations of 1, 3, or 7 days, under controlled temperature and humidity conditions. After an overnight fast, liver tissues were collected for histopathological, proteomic, and metabolomic analyses as described in Fig. 1A. Food and water consumption, as well as body weight, showed significant decreases after 7 days of hypobaric hypoxia exposure (Fig. 1B). Notably, AST and ALT levels showed mild elevations alongside a marked increase in hepatic fat accumulation and inflammatory neutrophil infiltration on day 7 (Fig. 1B and Fig. 1C).

Liver Metabolomics Revealed Distinct Hepatic Metabolic Alterations During Hypobaric Hypoxia.

The flowchart depicts the comprehensive experimental workflow encompassing hypoxia exposure, liver tissue collection, metabolomics analysis, and identification of differentially regulated metabolites (Figure-2A). Partial least squares discriminant analysis (PLS-DA) revealed a clear distinction between normoxic controls and hypoxia-exposed groups, underscoring significant changes in hepatic metabolic profiles following hypobaric hypoxia (Figure-2B). The progressive separation seen among Day 1, Day 3, and Day 7 cohorts shows duration-dependent metabolic adaptation during hypoxic stress. Heatmap analysis highlighted distinct patterns of metabolite expression across all experimental groups (Figure-2C). Differential metabolite analysis (Volcano plot) revealed pronounced metabolic perturbations corresponding to varying durations of hypoxia exposure. Specifically, Day 1 hypoxia resulted in 341 up- and 20 downregulated metabolites, Day 3 showed 316 upregulated and 22 downregulated metabolites; and Day 7 showed the greatest level of metabolic disruption with 356 upregulated and 31 downregulated metabolites (Figure-2D). Venn diagrams showed that metabolites significantly upregulated under hypoxia were linked to methionine and cysteine metabolism, glutathione metabolism, thiamine metabolism, malate-aspartate shuttle, citrate cycle (TCA cycle), pyrimidine metabolism, and purine metabolism pathways (Figure-2E, $p < 0.05$). Conversely, downregulated metabolites were associated with taurine and hypotaurine metabolism, bile acid biosynthesis, histidine metabolism, beta-alanine metabolism, methyl histidine metabolism, and ammonia recycling pathways ($p < 0.05$) (Figure-2E). Mean decrease in accuracy analysis showed several metabolites correlating with hypoxia exposure (Figure-2F). Receiver operating characteristic (ROC) analysis showed high predictive accuracy for the selected metabolite panel in distinguishing hypoxia-exposed groups from controls, suggesting their potential as biomarkers for hypoxia-induced hepatic metabolic dysfunction (Figure-2F). In summary, these results show that hypobaric hypoxia induces significant, time-dependent metabolic reprogramming in rat liver tissue, characterized by alterations in amino acid metabolism, energy metabolism, redox equilibrium, nucleotide metabolism, and bile acid-associated metabolic pathways.

Liver Proteomics analysis Revealed Distinct Hepatic Metabolic Alterations During Hypobaric Hypoxia.

The flowchart depicts the study design, including a comparative analysis of liver proteins, identification of differential regulated proteins and their functional significance (Figure-3A). PLS-DA analysis showed clear separation between normoxic controls and groups exposed to hypoxia, highlighting notable changes in hepatic protein profiles after hypobaric hypoxia (Figure-3B). Hierarchical clustering revealed unique patterns of protein expression in each experimental group (Figure-3C). Differentially expressed proteins (Volcano plot) during hypoxia: Day 1 exposure led to 1091 up- and 331 downregulated proteins, Day 3 resulted in 1146 up- and 472 downregulated proteins, and Day 7 showed 453 up- and 606 downregulated proteins, reflecting progressive proteome changes with continued hypoxia ($FC > 1.5$, $p < 0.05$, $FDR < 0.01$, Figure-3D). Comparative pathway enrichment showed pathways affected by hypoxia the upregulated proteins were related to metabolic processes, oxidative phosphorylation, glutathione metabolism, fatty acid degradation, pyruvate and amino acid metabolism, pentose phosphate pathway, ribosome biogenesis, thermogenesis, carbon metabolism, proteasome activity, and several neurodegenerative disease pathways (Figure-3E, $p < 0.05$). Whereas the downregulated proteins were linked to lysosomal function, bile secretion, focal adhesion, actin cytoskeleton regulation, protein

digestion and absorption, extracellular matrix-receptor interactions, endocytosis, complement and coagulation cascades, and multiple amino acid metabolism pathways (valine, leucine, isoleucine degradation, tryptophan, histidine, and arginine biosynthesis, $p < 0.05$, Figure-3E) respectively. Analysis of mean decrease in accuracy pinpointed specific proteins associated with hypoxia (Figure-3F). ROC analyses showed robust predictive capability for the chosen protein panel with high AUC > 0.9,$p < 0.05$. Overall, liver proteomics results show that hypobaric hypoxia causes marked and time-dependent remodeling of the liver proteome, towards more pathogenic and inflammatory kind specifically influencing mitochondrial metabolism, oxidative stress response, amino acid and energy metabolisms, cytoskeletal structure, extracellular matrix regulation, platelet degranulation, neutrophil degradation, and hypoxia-related signal pathways.

Analysis of the liver proteome and metabolome shows that hypobaric hypoxia significantly affects inflammation, oxidative stress, angiogenesis, and lipid metabolism.

To understand the metabolic disturbances linked to hypobaric hypoxia (associated with temporal disease progression). The proteomics and metabolomics data were subjected to integration analysis (Figure-4A). We used two independent strategies to integrate the multi-omics data. 1) for temporal integration: The proteomics and metabolomics data was subjected to correl analysis (day1 to day 7) to identify proteins and metabolites that correlate ($R2 > 0.7$, $p < 0.05$) with the days to exposure. We also performed weighted proteome /metabolome correlation network analysis (WP/MCNA) and show metabolite and proteins cluster specific to day of exposure (hypobaric hypoxia).

The correl analysis of proteomics and metabolomics shows temporal disease progression throughout hypoxia (Figure-4B). Proteins which positively correlated to the increase in hypobaric hypoxia condition were significantly linked to valine degradation, protein citrullination, post-translational modification, immune response, intracellular signaling, and metabolic processes and metabolomic enrichment analysis showed increased involvement of glutamate metabolism, purine metabolism, ketone body metabolism, tryptophan metabolism, phenylalanine metabolism, and amino acid metabolic pathways whereas proteins and metabolites which showed negative correlation with the temporal change in hypoxia exposure were linked to ammonia recycling, beta-alanine metabolism, histidine metabolism and other pathways (Figure-4C).

Multiomics integration using temporal association analysis and weighted protein co-expression network analysis (WGCNA) revealed distinct metabolite and protein modules, which were further connected through regulatory network mapping to identify functionally associated pathways. The mean cluster intensity (MCI) analysis demonstrated temporal changes in both proteomic and metabolomic datasets from Day 0 to Day 7 of hypoxia exposure (Fig. 4D).

Distinct clustering patterns among metabolomic and proteomic modules across different time points were identified, Day 7 hypoxia was specific to MEblue module for the metabolite and MEgreen, MEblack, MEmegenta, MEyello, and MEblue for the protein module respectively (Fig. 4D).

The identified metabolite and proteins modules were cross correlated to identified proteins and metabolite integration and linked pathways. We observed strong positive and negative associations among proteomic and metabolomic modules (Figure-4E). MEblue module for the metabolite showed strong correlation with MEgreen, MEblack, MEmegenta, MEyello, and MEblue for the protein module specific to day 7, integrated network analysis of these module showed significant correlation of the metabolites and proteins linked to amino acid metabolism, platelet activation, angiogenesis, apoptosis, EGFR signaling, and lipid metabolism (Fig. 4F). Key metabolites including pyruvate, glutamate, folate-associated metabolites, betaine aldehyde, and amino acid intermediates displayed strong associations with proteins linked to platelet activation, apoptosis signaling, and metabolic regulation. These findings shows that hypobaric hypoxia even by day 7 induces coordinated proteomic and metabolomic remodeling, associated to induction of apoptosis, inflammatory and oxidative changes, which contributes to significant increase in the lipid accumulation in the liver (metabolic stress) and thus induces molecular derangement in the liver (Fig. 4F). These pathways are crucial and warrants validation and association to pathological transformation due to hypoxia.

Discussion:

Hypobaric hypoxia is marked by reduced pressure and oxygen, affects both gut and brain function (1). It alters gut metabolism, impacting nutrient absorption and digestion, in addition the brain faces oxidative changes, which may impair cognition. These effects show hypobaric hypoxia's role in multi-organ dysfunction beyond liver injury (2, 3). The liver is particularly susceptible to oxygen deprivation because of its high metabolic activity and dependence on mitochondrial oxidative phosphorylation for maintenance of cellular energy homeostasis (4).

In this study, rats were subjected to hypobaric hypoxia for seven days, after which physiological, biochemical, histopathological, metabolomic, proteomic, and molecular alterations in liver tissue were assessed. Exposure to hypobaric hypoxia resulted in a significant decrease in body weight and food intake, indicating a disruption in systemic energy balance under oxygen-deficient conditions. These findings are consistent with previous research demonstrating that hypoxia suppresses appetite and modifies nutrient utilization via hypoxia-inducible signaling pathways and neuroendocrine mechanisms (43). The combination of reduced caloric intake and heightened metabolic demand during hypoxic stress likely contributes to the observed impairment in body weight gain; similar decreases in body weight and feeding behavior have been documented in experimental high-altitude hypoxia models (43).

Biochemical analyses showed that serum AST and ALT levels increased after exposure to hypoxia, pointing to liver cell injury and compromised membrane integrity. Elevated transaminase activity is recognized as an indicator of liver damage linked to oxidative stress, mitochondrial dysfunction, and inflammation (44). Hypoxia impairs mitochondrial respiratory function, leading to excess reactive oxygen species (ROS), lipid peroxidation, and destabilized membranes, which causes intracellular enzymes to leak into the bloodstream (45). Continued rises in AST and ALT during extended hypoxia suggest

ongoing liver injury and worsening cellular health. Histopathological results using H&E staining revealed advancing hepatic steatosis, liver cell degeneration, sinusoidal dilation, inflammatory infiltration, and disrupted liver structure in groups exposed to hypoxia. This hypoxia-induced steatosis may be due to changes in lipid metabolism, defective mitochondrial β oxidation, oxidative stress, and HIF-driven activation of lipogenic pathways (46). Sirius Red (SR) staining also showed increasing collagen buildup and extracellular matrix accumulation in the livers exposed to hypoxia, marking the activation of fibrotic pathways under sustained low-oxygen conditions. Prior studies have shown that hypoxia activates hepatic stellate cells through HIF 1α signaling, ROS production, inflammatory cytokines, and TGF β pathways, resulting in more collagen synthesis and fibrotic changes (22, 47). Current proteomics data further confirm these findings, indicating altered extracellular matrix organization, focal adhesion, and cytoskeletal pathways, supporting evidence of structural remodeling in the liver during hypoxia.

Liver metabolomics analysis showed substantial hepatic metabolic reprogramming during exposure to hypobaric hypoxia. Multivariate statistical analyses indicated pronounced segregation between normoxia and hypoxia-treated groups, underscoring significant alterations in hepatic metabolic profiles resulting from oxygen deprivation. Comparable metabolic divergence has been documented in previous studies of chronic hypoxia (48). Differential metabolite analysis revealed significant enrichment in pathways including methionine and cysteine metabolism, glutathione metabolism, thiamine metabolism, malate-aspartate shuttle, citrate cycle, purine metabolism, and pyrimidine metabolism. Hypoxia-induced mitochondrial dysfunction is associated with impaired electron transport chain activity and increased ROS production, leading to oxidative stress and metabolic imbalance (49). The activation of glutathione metabolism observed represents a compensatory antioxidant response aimed at neutralizing excessive ROS accumulation and maintaining intracellular redox homeostasis. Enhanced methionine and cysteine metabolism further supports increased glutathione biosynthesis during hypoxic stress, as cysteine serves as the rate-limiting substrate for glutathione synthesis (50). Alterations in malate-aspartate shuttle and tricarboxylic acid cycle pathways suggest significant mitochondrial metabolic rewiring and impaired oxidative phosphorylation under oxygen-deficient conditions (51). Taurine and related metabolic pathways, as well as bile acid biosynthesis, beta alanine, histidine metabolism, and ammonia recycling, were downregulated under 7- days of hypoxia. Taurine is vital for membrane stability, mitochondrial function, calcium balance, and anti-oxidative defense; its suppression may increase vulnerability to oxidative damage and liver dysfunction (5).

Liver Proteomics analysis showed substantial alterations in hepatic protein expression, notably an upregulation of proteins related to glycolysis, the pentose phosphate pathway, and proteasome activity. These findings suggest mitochondrial dysfunction and an adaptive shift in cellular energy metabolism. Hypoxic conditions restrict mitochondrial respiration, increasing cellular dependence on glycolysis and activating protein quality control mechanisms such as the ubiquitin-proteasome system. The concurrent elevation of antioxidant and proteostasis-associated proteins shows a coordinated hepatic response to oxidative stress. Additionally, proteomic profiling revealed enrichment of pathways associated with mitochondrial dysfunction, oxidative stress, disrupted proteostasis, and metabolic imbalance, all of

which are common cellular outcomes of hypoxic injury (52). Earlier proteomics studies under chronic hypoxia (48) have reported similar enrichment of neurodegeneration-related molecular pathways.

Downregulated proteins observed in the present study were linked to lysosomal function, focal adhesion, extracellular matrix organization, actin cytoskeleton regulation, endocytosis, complement activation, and protein digestion and absorption processes. Hypoxia-induced disturbances of cytoskeletal architecture and extracellular matrix stability contribute to hepatic cell injury, vascular dysfunction, inflammation, and progression of fibrosis (53). Reduced expression of proteins involved in focal adhesion and cytoskeletal maintenance may compromise hepatic structural integrity during prolonged hypoxic exposure.

Integrated proteomic and metabolomic analyses showed proteins and metabolites that strongly correlate with increased hypoxia exposure, especially at Day 7. Positively correlated proteins were linked to amino acid metabolism, immune response, and intracellular signaling, while negatively correlated molecules were associated with ammonia recycling and histidine metabolism. Network mapping revealed distinct modules tied to apoptosis, angiogenesis, platelet activation, and lipid metabolism. Key metabolites like pyruvate and glutamate connected with protein markers for platelet activation and metabolic regulation. Overall, hypobaric hypoxia triggered coordinated molecular changes related to apoptosis, inflammation, oxidative stress, and lipid accumulation in the liver which warrants validation.

LCMS/MS, immune-histochemical, and RTPCR methods validated metabolites and proteins involved in relevant pathways. Caspase 3 showed increased expression in hypoxia-treated groups, signifying apoptotic activation. As a key mitochondrial protease, Caspase 3 is activated by oxidative stress, mitochondrial damage, inflammation, and cytochrome c release (54). Metabolomics and proteomics findings were substantiated by RT PCR and Caspase 3 immunohistochemistry, which showed significant changes in hypoxia-responsive genes linked to oxidative stress, inflammation, angiogenesis, mitochondrial dysfunction, and apoptosis. Collectively, the increase in apoptosis-related gene expression and Caspase 3 activity points to programmed cell death during hypoxia-induced liver injury.

Finally our study shows that short term hypobaric hypoxia causes progressive liver injury marked by metabolic dysfunction, oxidative stress, mitochondrial damage, inflammation, apoptosis, and changes in the extracellular matrix. Combined analyses offer detailed insight into liver adaptation and damage under ongoing low-oxygen conditions. These results point to key areas for further research and improvement in Hypoxia induced liver injury.

Integrated multiomics framework illustrating the molecular mechanisms underlying hypoxia-induced liver injury.

Male Sprague–Dawley rats were exposed to simulated hypobaric hypoxia equivalent to 25,000 ft for 1, 3, or 7 days, followed by comprehensive liver proteomic and metabolomic profiling. Integrated multiomics analysis revealed progressive **redox imbalance, metabolic rewiring, and inflammatory activation** in response to hypoxic exposure. Hypoxia-responsive signaling, oxidative stress, and metabolic alterations

converged on **Eph-ephrin signaling**, which was identified as a central regulatory pathway associated with inflammatory activation. Key molecular alterations involved oxidative stress-related mediators (**SOD1, SOD2, NOX4**), hypoxia signaling (**HIF1A**), angiogenesis (**VEGF**), inflammatory mediators (**IL-6, TNF-α, NF-κB**), and metabolic pathways involving the **TCA cycle, amino acids, lipids, and bile acids**. Network analysis demonstrated interactions between Eph-ephrin signaling and oxidative stress, angiogenesis, inflammation, and metabolic remodeling. These molecular alterations were associated with progressive hepatic injury and activation of the apoptotic pathway, as evidenced by increased **caspase-3** expression/activity. RT-PCR and immunohistochemical validation supported the identified pathway alterations. The proposed model suggests that **Eph-ephrin signaling represents a potential mechanistic link between hypoxia-induced metabolic/redox dysfunction and hepatic inflammation and apoptosis**, highlighting it as a potential therapeutic target for hypoxia-associated liver injury.

Author Contribution

Authors' contributions: JSM and NS conceptualized the work. Samples were provided by SY and RK. SY and RK were responsible for sample processing and experimental work, analysis and manuscript writing and drafting and were helped by GT, NS,SP,VS,VB,YM,SA for helping in experimenattion. Data analysis was performed by SY under the guidance of JSM,NS,VPD,NKS. The manuscript was drafted by SY and RK and reviewd by JSM and NS. This manuscript has been seen and approved by all authors.

Acknowledgments-

The work was supported by LSRB, Defence Research and Development Organisation (DRDO)

All experimental procedures were performed in accordance with the guidelines of the Institutional Animal Ethics Committee guidelines for the care and use of laboratory animals institute is Banasthali Vidyapith University, approved ethical committee Bioscience & Biotechnology, Banasthali vidyapith, Rajasthan & ethical number BV/IAEC/2023/4643.

Data Availability

All the analyzed data had been provided in manuscript and the raw data is available upon request to corresponding author.

References

1. Kanehisa, M. & Goto, S. KEGG: kyoto encyclopedia of genes and genomes. *Nucleic Acids Res.* **28**, 27–30 (2000).

2. West, J. B. IX World Congress on High Altitude Medicine and Physiology, Taipei, Taiwan, November 3–6, 2012. *High. Alt Med. Biol.* **13** (3), 140 (2012).
3. Nath, B. & Szabo, G. Hypoxia and hypoxia inducible factors: diverse roles in liver diseases. *Hepatology* **55** (2), 622–633 (2012).
4. West, J. B., American College of P & American Physiological, S. The physiologic basis of high-altitude diseases. *Ann. Intern. Med.* **141** (10), 789–800 (2004).
5. Debevec, T. & Millet, G. P. Discerning normobaric and hypobaric hypoxia: significance of exposure duration. *J. Appl. Physiol. (1985)*. **116** (9), 1255 (2014).
6. Kung-Chun Chiu, D. et al. Hypoxia regulates the mitochondrial activity of hepatocellular carcinoma cells through HIF/HEY1/PINK1 pathway. *Cell. Death Dis.* **10** (12), 934 (2019).
7. Schieber, M. & Chandel, N. S. ROS function in redox signaling and oxidative stress. *Curr. Biol.* **24** (10), R453–R462 (2014).
8. Xu, Z. et al. Transcriptional profiling in the livers of rats after hypobaric hypoxia exposure. *PeerJ* **7**, e6499 (2019).
9. Wang, G. L. & Semenza, G. L. General involvement of hypoxia-inducible factor 1 in transcriptional response to hypoxia. *Proc. Natl. Acad. Sci. U S A*. **90** (9), 4304–4308 (1993).
10. Whitmer, J. T., Idell-Wenger, J. A., Rovetto, M. J. & Neely, J. R. Control of fatty acid metabolism in ischemic and hypoxic hearts. *J. Biol. Chem.* **253** (12), 4305–4309 (1978).
11. Papandreou, I., Cairns, R. A., Fontana, L., Lim, A. L. & Denko, N. C. HIF-1 mediates adaptation to hypoxia by actively downregulating mitochondrial oxygen consumption. *Cell. Metab.* **3** (3), 187–197 (2006).
12. Yang, Z. et al. HIF-2alpha-driven Lipogenesis and Inflammation in Metabolic Dysfunction-associated Steatotic Liver Disease: Role of ATF4 Signaling. *Cell. Mol. Gastroenterol. Hepatol.* **20** (2), 101651 (2026).
13. Mylonis, I., Simos, G. & Paraskeva, E. Hypoxia-Inducible Factors and the Regulation of Lipid Metabolism. *Cells* ;**8**(3). (2019).
14. Bingol, K. Recent Advances in Targeted and Untargeted Metabolomics by NMR and MS/NMR Methods. *High. Throughput* ;**7**(2). (2018).
15. Fuhrmann, D. C. & Brune, B. Mitochondrial composition and function under the control of hypoxia. *Redox Biol.* **12**, 208–215 (2017).
16. Solanki, S. & Shah, Y. M. Hypoxia-Induced Signaling in Gut and Liver Pathobiology. *Annu. Rev. Pathol.* **19**, 291–317 (2024).
17. Fridovich, I. Superoxide dismutases: defence against endogenous superoxide radical. Ciba Found Symp. (65):77–93. (1978).
18. Oliver, K. M., Taylor, C. T. & Cummins, E. P. Hypoxia. Regulation of NFkappaB signalling during inflammation: the role of hydroxylases. *Arthritis Res. Ther.* **11** (1), 215 (2009).

19. Larche, M., Akdis, C. A. & Valenta, R. Immunological mechanisms of allergen-specific immunotherapy. *Nat. Rev. Immunol.* **6** (10), 761–771 (2006).
20. Viscor, G. et al. Physiological and Biological Responses to Short-Term Intermittent Hypobaric Hypoxia Exposure: From Sports and Mountain Medicine to New Biomedical Applications. *Front. Physiol.* **9**, 814 (2018).
21. Virues-Ortega, J., Buela-Casal, G., Garrido, E. & Alcazar, B. Neuropsychological functioning associated with high-altitude exposure. *Neuropsychol. Rev.* **14** (4), 197–224 (2004).
22. Friedman, S. L. Mechanisms of hepatic fibrogenesis. *Gastroenterology* **134** (6), 1655–1669 (2008).
23. Wellen, K. E. & Hotamisligil, G. S. Inflammation, stress, and diabetes. *J. Clin. Invest.* **115** (5), 1111–1119 (2005).
24. Wang, K. Molecular mechanisms of hepatic apoptosis. *Cell. Death Dis.* **5** (1), e996 (2014).
25. Church, R. J. & Watkins, P. B. The transformation in biomarker detection and management of drug-induced liver injury. *Liver Int.* **37** (11), 1582–1590 (2017).
26. Chen, L. D. et al. Untargeted Metabolomic Profiling of Liver in a Chronic Intermittent Hypoxia Mouse Model. *Front. Physiol.* **12**, 701035 (2021).
27. Gao, Z., Luo, G. & Ni, B. Progress in Mass Spectrometry-Based Proteomics in Hypoxia-Related Diseases and High-Altitude Medicine. *OMICS* **21** (6), 305–313 (2017).
28. Pasquale, E. B. Eph receptors and ephrins in cancer: bidirectional signalling and beyond. *Nat. Rev. Cancer*. **10** (3), 165–180 (2010).
29. Kullander, K. & Klein, R. Mechanisms and functions of Eph and ephrin signalling. *Nat. Rev. Mol. Cell. Biol.* **3** (7), 475–486 (2002).
30. Patti, G. J., Yanes, O., Siuzdak, G. & Innovation Metabolomics: the apogee of the omics trilogy. *Nat. Rev. Mol. Cell. Biol.* **13** (4), 263–269 (2012).
31. Zwaans, B. M. & Lombard, D. B. Interplay between sirtuins, MYC and hypoxia-inducible factor in cancer-associated metabolic reprogramming. *Dis. Model. Mech.* **7** (9), 1023–1032 (2014).
32. Hodson, L., Humphreys, S. M., Karpe, F. & Frayn, K. N. Metabolic signatures of human adipose tissue hypoxia in obesity. *Diabetes* **62** (5), 1417–1425 (2013).
33. Hu, B. et al. A comprehensive characterization of metabolic signatures-hypoxia, glycolysis, and lactylation-in non-healing diabetic foot ulcers. *Front. Mol. Biosci.* **12**, 1593390 (2025).
34. Jiang, L. et al. Localized hypoxia results in spatially heterogeneous metabolic signatures in breast tumor models. *Neoplasia* **14** (8), 732–741 (2012).
35. Ackerman, D. & Simon, M. C. Hypoxia, lipids, and cancer: surviving the harsh tumor microenvironment. *Trends Cell. Biol.* **24** (8), 472–478 (2014).
36. Taylor, C. T. & Scholz, C. C. The effect of HIF on metabolism and immunity. *Nat. Rev. Nephrol.* **18** (9), 573–587 (2022).
37. Sadiku, P. & Walmsley, S. R. Hypoxia and the regulation of myeloid cell metabolic imprinting: consequences for the inflammatory response. *EMBO Rep.* ;**20**(5). (2019).

38. Xu, J. et al. A global view on quantitative proteomic and metabolic analysis of rat livers under different hypoxia protocols. *Heliyon* **10** (19), e37791 (2024).
39. Jiang, X., Chen, S., Zhu, M. & Wu, C. Global Xenobiotic Profiling of Rat Plasma Using Untargeted Metabolomics and Background Subtraction-Based Approaches: Method Evaluation and Comparison. *Curr. Drug Metab.* **24** (3), 200–210 (2023).
40. Li, N. et al. The multiple organs insult and compensation mechanism in mice exposed to hypobaric hypoxia. *Cell. Stress Chaperones*. **25** (5), 779–791 (2020).
41. Prabhakar, N. R. & Kumar, G. K. Oxidative stress in the systemic and cellular responses to intermittent hypoxia. *Biol. Chem.* **385** (3–4), 217–221 (2004).
42. Yingzhong, Y., Droma, Y., Rili, G. & Kubo, K. Regulation of body weight by leptin, with special reference to hypoxia-induced regulation. *Intern. Med.* **45** (16), 941–946 (2006).
43. Mortola, J. P., Matsuoka, T., Saiki, C. & Naso, L. Metabolism and ventilation in hypoxic rats: effect of body mass. *Respir Physiol.* **97** (2), 225–234 (1994).
44. Giannini, E. G., Testa, R. & Savarino, V. Liver enzyme alteration: a guide for clinicians. *CMAJ* **172** (3), 367–379 (2005).
45. Chandel, N. S. et al. Reactive oxygen species generated at mitochondrial complex III stabilize hypoxia-inducible factor-1alpha during hypoxia: a mechanism of O2 sensing. *J. Biol. Chem.* **275** (33), 25130–25138 (2000).
46. Huang, D. et al. HIF-1-mediated suppression of acyl-CoA dehydrogenases and fatty acid oxidation is critical for cancer progression. *Cell. Rep.* **8** (6), 1930–1942 (2014).
47. Wang, Y. et al. Hypoxia-inducible factor-1alpha and MAPK co-regulate activation of hepatic stellate cells upon hypoxia stimulation. *PLoS One*. **8** (9), e74051 (2013).
48. Liang, H. & Song, K. Comprehensive metabolomics and transcriptomics analysis reveals protein and amino acid metabolic characteristics in liver tissue under chronic hypoxia. *PLoS One*. **18** (9), e0291798 (2023).
49. Semenza, G. L. HIF-1 mediates metabolic responses to intratumoral hypoxia and oncogenic mutations. *J. Clin. Invest.* **123** (9), 3664–3671 (2013).
50. Lu, S. C. Glutathione synthesis. *Biochim. Biophys. Acta*. **1830** (5), 3143–3153 (2013).
51. Du, H., Xu, T., Yu, S., Wu, S. & Zhang, J. Mitochondrial metabolism and cancer therapeutic innovation. *Signal. Transduct. Target. Ther.* **10** (1), 245 (2025).
52. Lin, M. T. & Beal, M. F. Mitochondrial dysfunction and oxidative stress in neurodegenerative diseases. *Nature* **443** (7113), 787–795 (2006).
53. Wiafe, B. et al. Hypoxia-increased expression of genes involved in inflammation, dedifferentiation, pro-fibrosis, and extracellular matrix remodeling of human bladder smooth muscle cells. *Vitro Cell. Dev. Biol. Anim.* **53** (1), 58–66 (2017).
54. Elmore, S. Apoptosis: a review of programmed cell death. *Toxicol. Pathol.* **35** (4), 495–516 (2007).
55. Legend.

Figures

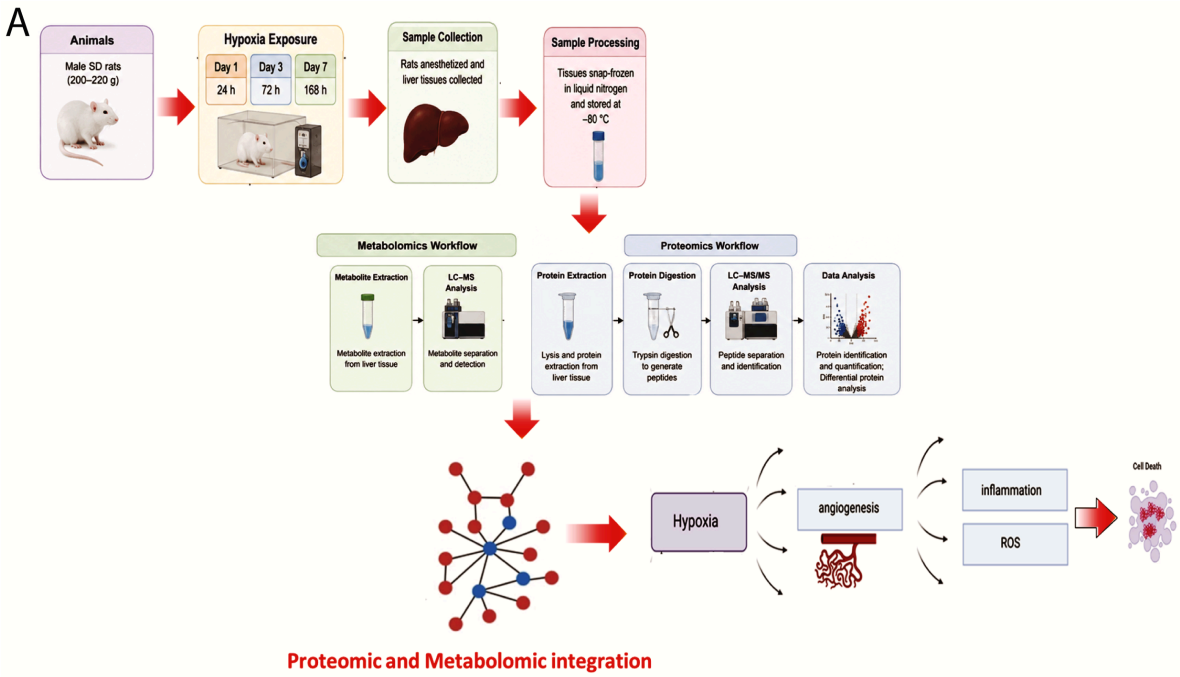

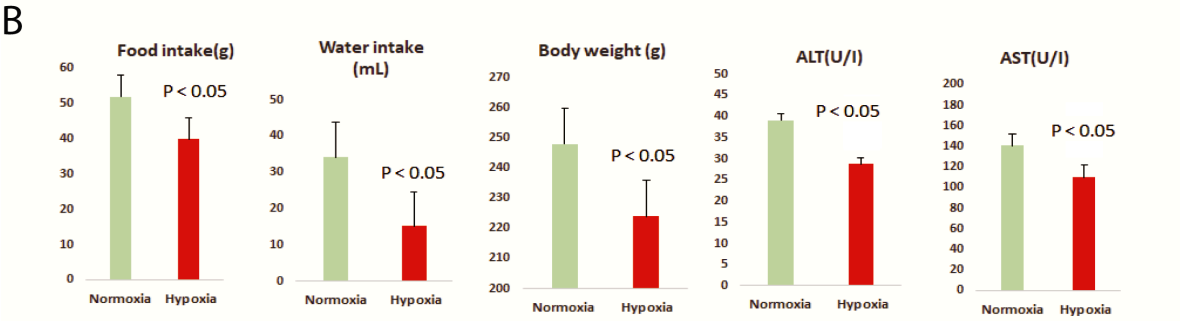

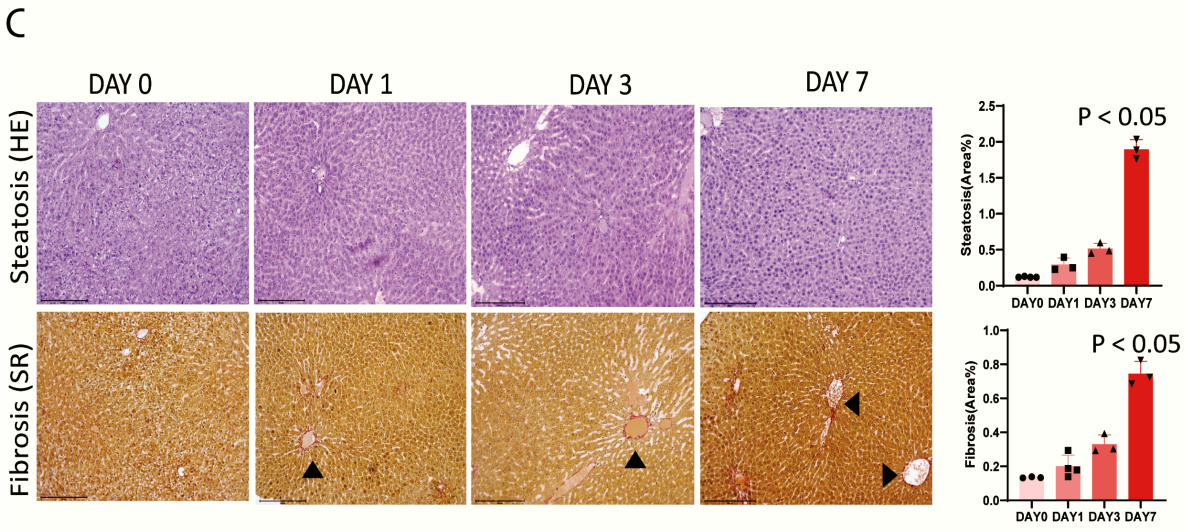

Figure 1

Experimental design and characterization of hypobaric hypoxia-induced liver injury.

(A) Experimental workflow for multi-omics profiling of hypobaric hypoxia-induced liver injury.

(B) Physiological and biochemical changes following hypobaric hypoxia exposure shows reduced food intake, water intake, and body weight with marginal increase in alanine aminotransferase (ALT) and aspartate aminotransferase (AST), together indicating progressive hepatocellular injury ($P < 0.05$).

(C) Histopathological assessment of hypoxia-induced liver injury. Representative hematoxylin and eosin (H&E)-stained liver sections (10x) demonstrate progressive hepatic steatosis following hypobaric hypoxia exposure from Day 1 to Day 7. Sirius Red (SR)-stained sections reveal gradual collagen deposition surrounding portal and peri-sinusoidal regions, indicating the initiation of hepatic fibrogenesis shown by arrows ($P < 0.05$).

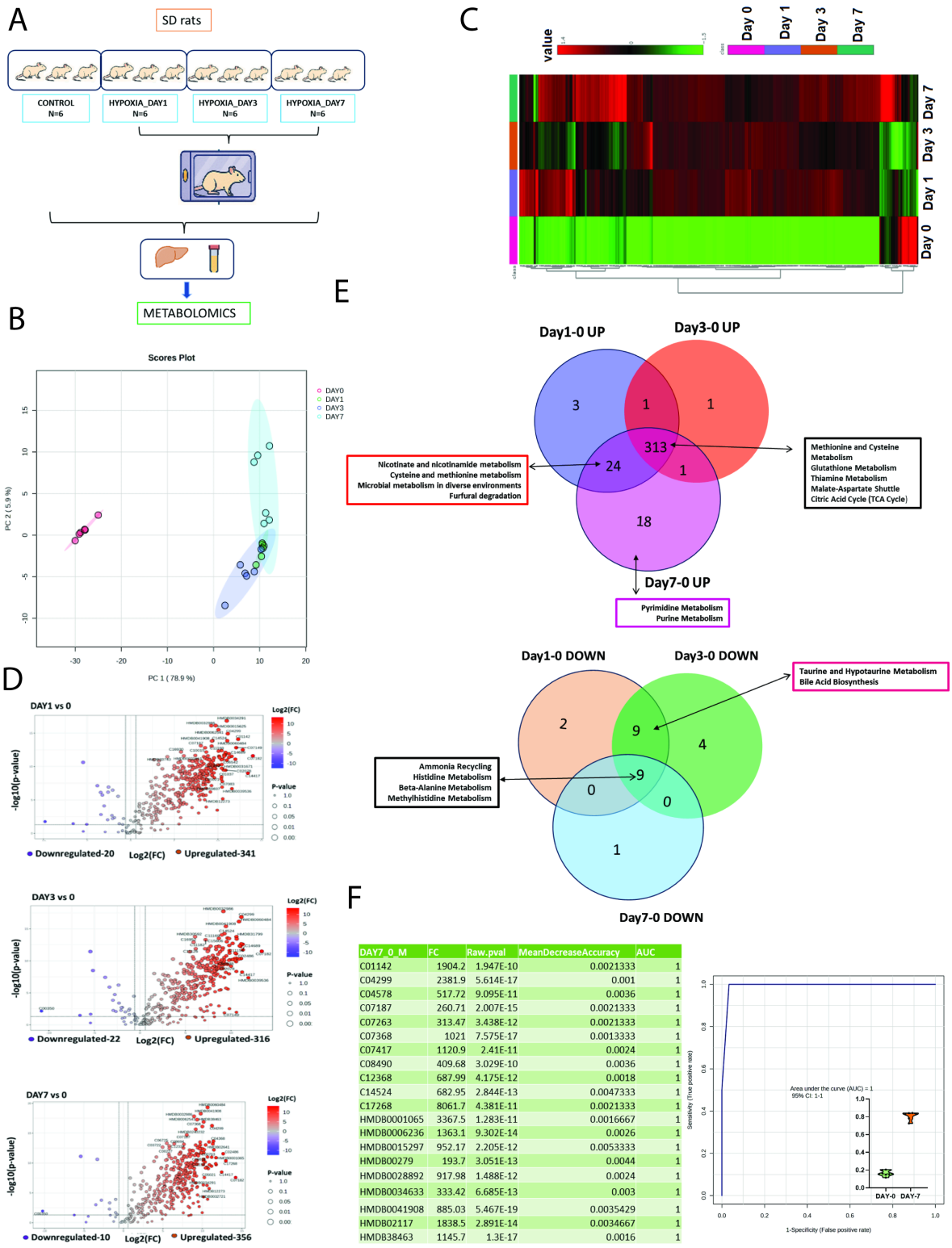

DAY7_0_M	FC	Raw.pval	MeanDecreaseAccuracy	AUC
C01142	1904.2	1.947E-10	0.0021333	1
C04299	2381.9	5.614E-17	0.001	1
C04578	517.72	9.095E-11	0.0036	1
C07187	260.71	2.007E-15	0.0021333	1
C07263	313.47	3.438E-12	0.0021333	1
C07368	1021	7.575E-17	0.0013333	1
C07417	1120.9	2.41E-11	0.0024	1
C08490	409.68	3.029E-10	0.0036	1
C12368	687.99	4.175E-12	0.0018	1
C14524	682.95	2.844E-13	0.0047333	1
C17268	8061.7	4.381E-11	0.0021333	1
HMDB0001065	3367.5	1.283E-11	0.0016667	1
HMDB0006236	1363.1	9.302E-14	0.0026	1
HMDB0015297	952.17	2.205E-12	0.0053333	1
HMDB00279	193.7	3.051E-13	0.0044	1
HMDB0028892	917.98	1.488E-12	0.0024	1
HMDB0034633	333.42	6.685E-13	0.003	1
HMDB0041908	885.03	5.467E-19	0.0035429	1
HMDB02117	1838.5	2.891E-14	0.0034667	1
HMDB38463	1145.7	1.3E-17	0.0016	1

Figure 2

Metabolomic profiling for estimating progressive effect of hypobaric hypoxia on differential metabolites in rat livers.

(A) Experimental design for untargeted liver metabolomics. SD rats were divided into control (Day 0) and hypobaric hypoxia groups (Day 1, Day 3, and Day 7; n = 6/group), followed by LC–MS-based metabolomic

profiling of liver tissues.

(B) Partial least squares-discriminant analysis (PLS-DA) score plot showing segregation of Hypoxia vs Normoxia (Hypoxia Day 1, Day 3, Day 7 Vs Day 0 Normoxia, based on metabolome profile ($p < 0.05$; Kruskal-Wallis test).

(C) Clustering heatmap of significantly altered metabolites. Heatmap visualization of differentially abundant metabolites across all experimental groups reveals distinct temporal metabolic signatures.

(D) Volcano plot analysis of differential metabolites. Volcano plots comparing Day 1, Day 3, and Day7 hypoxia groups with normoxia controls illustrate significantly altered metabolites based on fold change and statistical significance. Red dots represent significantly upregulated metabolites, blue dots represent significantly downregulated metabolites, and gray dots indicate metabolites without significant changes (F.C. >1.5, $p < 0.05$ considered significant).

(E) Venn diagram showing enrichment of upregulated pathways and downregulated pathways. Temporal overlap of differentially regulated metabolites and pathway enrichment analysis. Venn diagrams illustrate shared and unique upregulated and downregulated metabolites among Day 1, Day 3, and Day 7 following hypobaric hypoxia.

(F) Top 20 metabolites and their Mean decrease in accuracy analysis followed by Receiver operating characteristic (ROC) analysis showed high predictive accuracy for the top 20 selected metabolite panel distinguishing hypoxia-exposed groups from controls, suggesting their potential as biomarkers for hypoxia-induced hepatic metabolic dysfunction

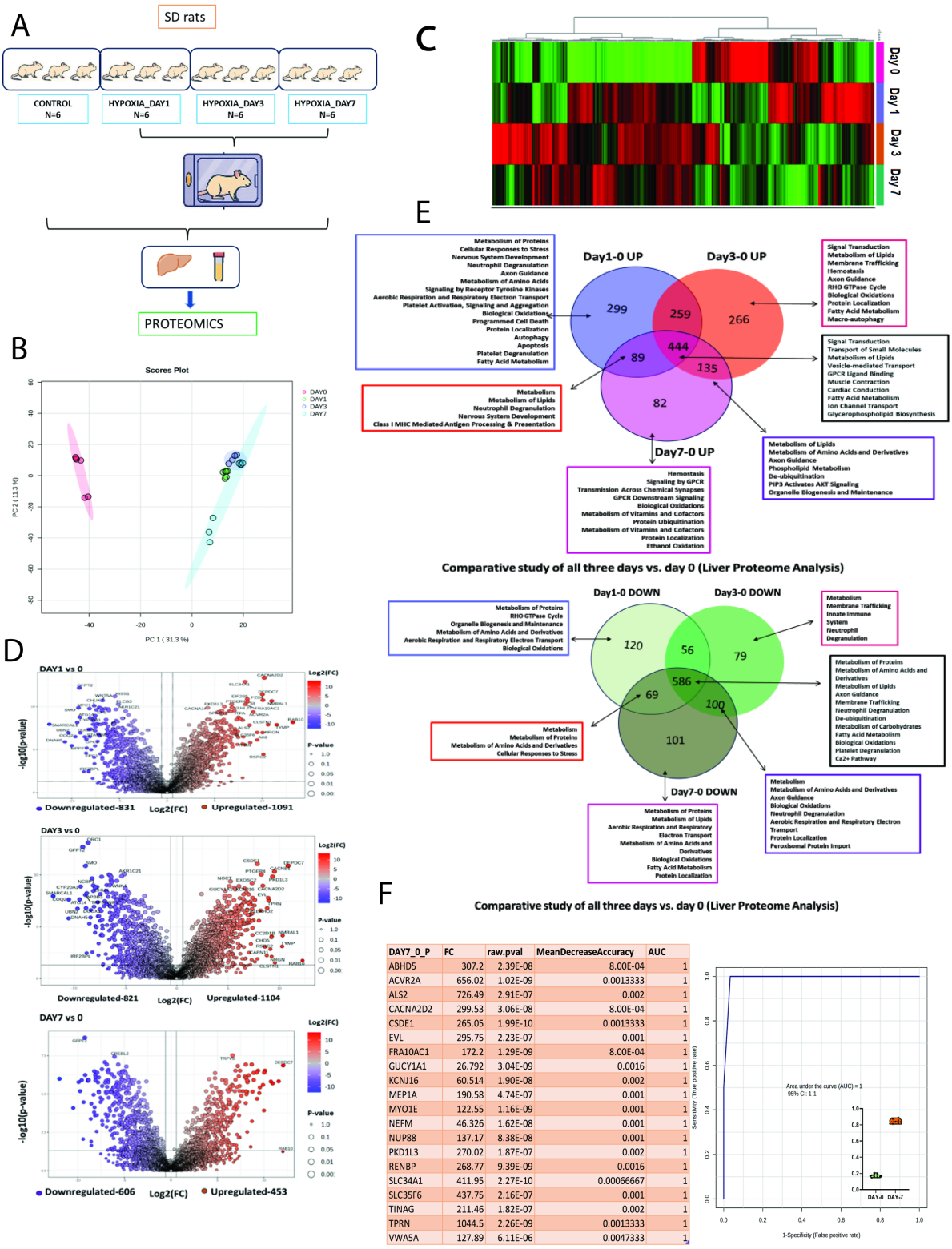

DAY7_0_P	FC	raw.pval	MeanDecreaseAccuracy	AUC
ABHD5	307.2	2.39E-08	8.00E-04	1
ACVR2A	656.02	1.02E-09	0.0013333	1
ALS2	726.49	2.91E-07	0.002	1
CACNA2D2	299.53	3.06E-08	8.00E-04	1
CSDE1	265.05	1.99E-10	0.0013333	1
EVL	295.75	2.23E-07	0.001	1
FRA10AC1	172.2	1.29E-09	8.00E-04	1
GUCY1A1	26.792	3.04E-09	0.0016	1
KCNJ16	60.514	1.90E-08	0.002	1
MEP1A	190.58	4.74E-07	0.001	1
MYO1E	122.55	1.16E-09	0.001	1
NEFM	46.326	1.62E-08	0.001	1
NUP88	137.17	8.38E-08	0.001	1
PKD1L3	270.02	1.87E-07	0.002	1
RENBP	268.77	9.39E-09	0.0016	1
SLC34A1	411.95	2.27E-10	0.00066667	1
SLC35F6	437.75	2.16E-07	0.001	1
TINAG	211.46	1.82E-07	0.002	1
TPRN	1044.5	2.26E-09	0.0013333	1
VWA5A	127.89	6.11E-06	0.0047333	1

Figure 3

Quantitative proteomic profiling reveals progressive molecular remodeling linked to inflammation and fibrosis in rat liver during hypobaric hypoxia.

(A) Experimental design for untargeted liver proteomics. SD rats were divided into control (Day 0) and hypobaric hypoxia groups (Day 1, Day 3, and Day 7; n = 6/group), followed by LC-MS-based metabolomic

profiling of liver tissues.

(B) Partial least squares-discriminant analysis (PLS-DA) score plot showing segregation of Hypoxia vs Normoxia (Hypoxia Day 1, Day 3, Day 7 Vs Day 0 Normoxia, based on proteome profile ($p < 0.05$; Kruskal-Wallis test).

(C) Clustering heatmap of differentially expressed proteins. Heatmap visualization of significantly altered proteins across Day 0, Day 1, Day 3, and Day 7 demonstrates distinct temporal expression patterns during hypobaric hypoxia, highlights progressive proteomic reprogramming with increasing duration of hypoxia exposure.

(D) Volcano plots comparing Day 1, Day 3, and Day 7 with normoxia controls identify significantly regulated proteins based on fold-change and statistical significance. Red dots represent significantly upregulated proteins, blue dots represent significantly downregulated proteins, and gray dots represent proteins without significant differential expression (F.C. >1.5, $p < 0.05$ considered significant).

(E) Venn diagram showing enrichment of upregulated pathways and downregulated pathways. Temporal overlap of differentially regulated proteins and pathway enrichment analysis. Venn diagrams illustrate shared and unique upregulated and downregulated proteins among Day 1, Day 3, and Day 7 following hypobaric hypoxia.

(F) Top 20 proteins and their mean decrease in accuracy followed by ROC analyses showed robust predictive capability of the protein panel with high AUC>0.9,p<0.05.

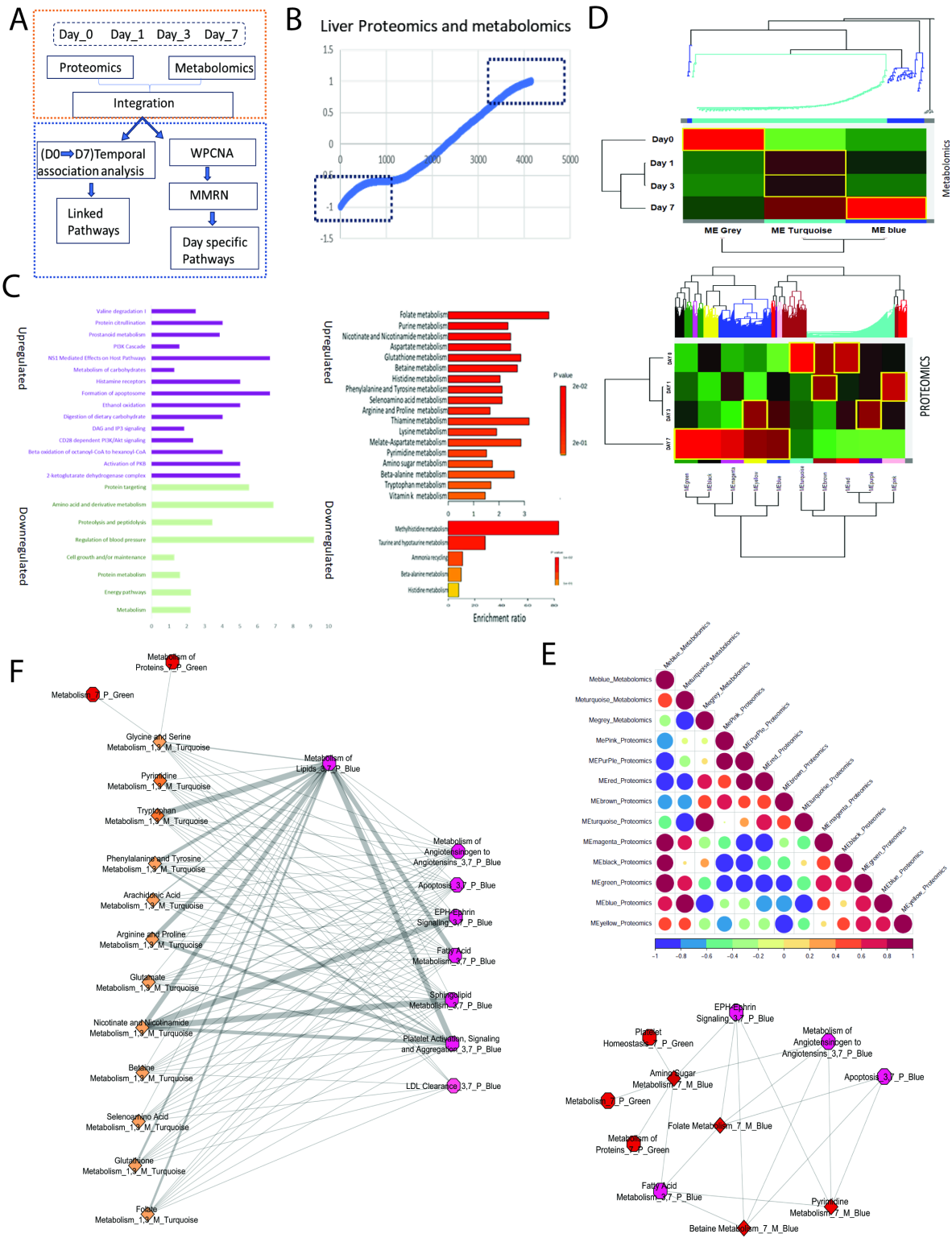

Figure 4

Integrated proteomic and metabolomic network analysis reveals coordinated molecular alterations during hypobaric hypoxia-induced liver injury.

(A) Schematic overview of the integrative multi-omics workflow illustrating temporal association analysis, weighted protein co-expression network analysis (WPCNA), module-module relationship

network (MMRN) construction, and identification of linked and day-specific biological pathways from liver proteomic and metabolomic datasets.

(B) Correlation analysis between liver proteomic and metabolomic datasets demonstrating the global association between differentially expressed proteins and metabolites across all experimental groups.

(C) Functional enrichment analysis of significantly upregulated and downregulated integrated pathways identified following hypobaric hypoxia exposure. Pathway enrichment was performed using differentially expressed proteins and metabolites obtained from integrated multi-omics analysis.

(D) WGPNA and WMCNA based Hierarchical clustering maps of significantly associated metabolomic and proteomic co-expression modules identified by weighted network analysis across Day 0, Day 1, Day 3, and Day 7 experimental groups.

(E) Correlation matrix illustrating the relationships between metabolomic and proteomic co-expression modules identified by weighted network analysis

(F) Integrated module-pathway interaction networks depicting associations between metabolomic modules, proteomic modules, and significantly enriched biological pathways identified through multi-omics integration.

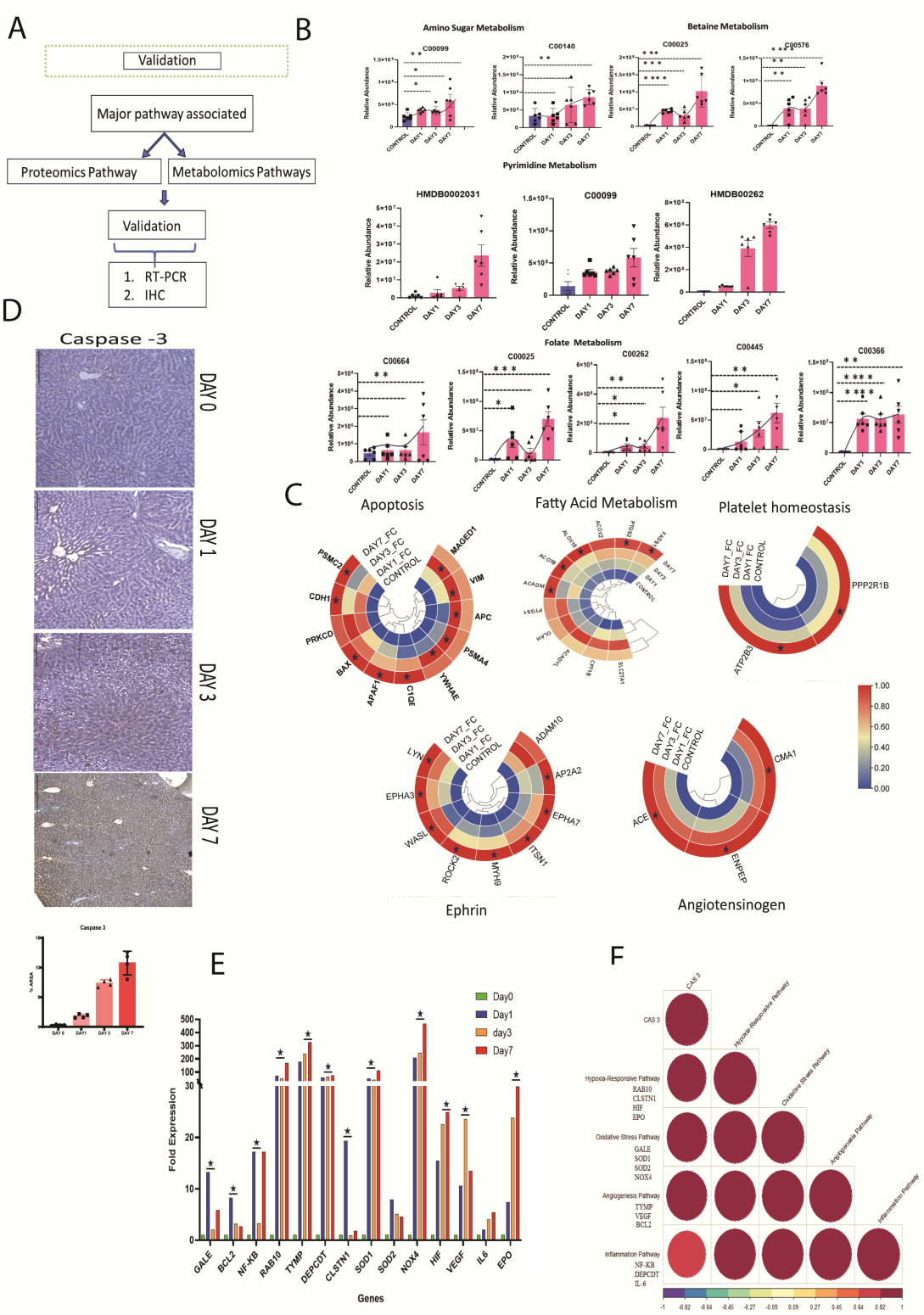

Figure 5

Multi-platform validation of integrated proteomic and metabolomic pathways identifies hypobaric hypoxia-induced molecular signatures associated with hepatic injury, angiogenesis, and apoptosis.

(A) Schematic representation of the validation workflow employed following integrative proteomic and metabolomic analyses.

(B) Experimental validation of significantly altered metabolites associated with key metabolic pathways. Relative abundances of representative across Day 0, Day 1, Day 3, and Day 7 hypobaric hypoxia exposure ($P < 0.05$).

(C) Circular heatmap depicting expression profiles of proteins associated with validated biological pathways Relative abundances of representative across Day 0, Day 1, Day 3, and Day 7 hypobaric hypoxia exposure ($P < 0.05$).

(D) Immunohistochemical validation of Caspase-3 expression. Representative immunohistochemical staining of liver sections demonstrates progressive increases in Caspase-3 expression following hypobaric hypoxia exposure from Day 1 through Day 7 compared with normoxia controls ($P < 0.05$).

(E) Quantitative RT-qPCR validation of representative genes identified through integrated pathway analysis.

(F) Integrated pathway correlation analysis of validated molecular signatures.

Supplementary Files

This is a list of supplementary files associated with this preprint. Click to download.

- GraphicalAbstract.jpg